

## Theory of light-induced drift. I. Flat-plate geometry

Frank O. Goodman\*

*Department of Applied Mathematics, University of Waterloo, Waterloo, Ontario, Canada N2L 3G1*

(Received 1 May 2001; published 17 June 2002)

Light-induced drift (LID) of a rarefied gas in a cell with flat-plate geometry is studied in the limits of large length and width of the cell, and exact solutions to the model rate equations are obtained, with exact analytical solutions for the case of surface LID (SLID); the special case of the limit of low radiation absorption by the gas in SLID is given particular attention. Many results are different from those of previous work. Emphasis is placed on considerations of comparison with experiment.

DOI: 10.1103/PhysRevA.65.063409

PACS number(s): 34.50.Rk

### I. INTRODUCTION

It seems that the phenomenon of light-induced drift (LID) was first predicted theoretically by Gelmukhanov and Shalagin [1,2] about two decades ago. They studied the effect now called BLID, which stands for bulk LID and is a drift effect that originates in the bulk of a gas in the possible absence of gas-wall effects. SLID, which stands for surface LID and which originates at the walls of a gas cell in the possible absence of bulk effects, was first predicted by Ghiner, Stockmann and Vaksman [3]; since then, a mixed LID effect has been predicted by Vaksman [4], BLID investigated by Ghiner and Vaksman [5], and SLID discussed in several publications [6–11].

The LID effect is essentially the following. A laser beam passes through a closed cell containing a rarefied gas, one component of which consists of excitable gas molecules (we use the terminology “molecules” for the active gas components), and the laser is tuned to excite molecules in a chosen velocity interval. The interaction properties of excited-state and ground-state molecules with other (buffer) particles in the bulk of the gas and/or with the cell walls, usually modeled in LID theory by bulk and surface “accommodation coefficients,” may be different, in which case LID may manifest itself by an initial drift of molecules, one way or the other, parallel to the laser beam. Because the gas cell is closed, molecules cannot drift in steady state, and a partial pressure difference builds up across the gas cell. This partial pressure difference is the main experimental manifestation of the LID effect, and is studied as a function of laser radiation intensity absorbed by the gas, although not presented in that manner, as we explain in Sec. VI. Experiments so far have been done for cases of low radiation intensity absorption in cells with circular-cylindrical (CC) and flat-plate (FP) geometries. This paper, part I of this series of papers, is restricted to FP geometry, in the limit of large cell length and cell width, and in the free-molecule limit.

Good qualitative explanations of the detailed physics behind the SLID effect have been given several times, for example, in Refs. [5,6,9,10], and there is no need to give another here. Experiments on SLID were first reported by

Hoogeveen, Spreeuw, and Hermans [12], with the first BLID experiments reported earlier (see Ref. [12] for references), all with CC geometry, and we refer to later CC [13–15] and FP [14,16] experiments. Reference should be made to the work of Chernyak, Vintovkina, and Chermyaninov [17] and of Zhdanov, Krylov, and Roldugin [18], who provide mathematically involved treatments of the kinetic equations for LID, with appropriate boundary conditions, and relate their results to those of Hoogeveen and co-workers [12–16].

Theoretical models have usually been so-called strong-collision Maxwell-Boltzmann-type models, involving parameters such as accommodation coefficients and decay rates, all of which are explained below. Previous treatments have a disadvantage, however, in that, having set up the model equations, approximations are made, most of which may well be justified, although the effects of these approximations are not always clear, at least to the present author. Just a single example should suffice here, and that is the prediction, made for FP geometry in Eq. (17) of Ref. [8], of a logarithmic singularity (diverging for large cell length/thickness ratio) in a certain SLID effect, which we conclude is wrong, although the origin of the incorrect result is by no means clear, and we conclude that it must lie in the subtle results of the seemingly reasonable, and certainly seemingly harmless, approximations made therein.

Within the same model framework as used previously, the intention of the present paper is to obtain exact results, both numerical and analytical, as far as is mathematically possible, of the LID effects with FP geometry in the stated limits. By “exact results” is meant results correct to arbitrary accuracy with no approximations (other than the setting up of the perforce approximate rate equations, of course) being made. It turns out that exact analytical results are impossible to obtain in the general case of LID, but are possible in either pure BLID or pure SLID, whereas exact numerical results are always possible to obtain, but much more easily in either pure BLID or pure SLID, with the latter being the easier one.

It may be argued that having exact results for such an approximate model is unnecessary, particularly as experiments are done, for example, in a low-intensity limit, and as the model parameters, even if they reasonably represent reality, are known to usually less than one-digit accuracy. However, exact results for a model are always important in checking previous models and in making/checking new and more general models.

---

\*Also at Department of Physics, University of Waterloo and the Guelph-Waterloo Physics Institute.

Several fresh concepts and results are presented, and seven of the appendixes should be regarded as reference sections for use throughout the paper. Appendix A defines important integrals over the velocity distributions which arise. Appendix B presents the Maxwellian and diffuse velocity distributions. An important function,  $G(u)$ , of one variable  $u$ , without which our results could not be called exact analytical, is defined, and its relevant expansions are given [19] in Appendix D, and certain integrals which are needed for exact analytical solution in SLID are evaluated in Appendix E. Some exact results are presented in Appendices F and G, and a discussion of free-molecule-flow transition probabilities appears in Appendix H.

In Sec. II, we describe the model and set up the defining Maxwell-Boltzmann rate equations (MBREs); a detailed description is given because our MBREs are different from those used before. Our theoretical results are related to experimental measurements in Sec III. In Sec. IV, we describe the exact numerical solution of the MBREs, with two independent procedures for getting exact steady-state results. In Sec. V, we specialize to the case of pure SLID, for which an exact analytical solution is possible, and further specializations are made, motivated by previous work, particularly to cases of low radiation intensity absorption. Illustrative results are shown where deemed appropriate.

Although the author is not aware of extensive experimental data on the dependence of SLID on experimental quantities such as absorbed intensity, care is taken to relate results to possible future experimental measurements, and considerations of applications to experiments, that is, the FP data in Refs. [14,16] are presented in Sec. VI. Sec. VII is a brief conclusion.

## II. DESCRIPTION OF THE MODEL AND DERIVATION OF THE MAXWELL-BOLTZMANN RATE EQUATIONS

Although in the present paper, calculations are made only for the case of pure SLID, the general case of LID is considered here for ease of reference in future publications. We consider the problem of LID in a rarefied gas containing two-level molecules with equal statistical level weights. The levels are denoted as is customary by subscripts ( $g, e$ )  $\equiv$  (ground, excited). The analysis is done using dimensional quantities at first, with dimensionless quantities introduced later. When BLID is involved, a model in two-dimensional (2D) space may be made [20], as it has considerable computational advantages over that in 3D space; for pure BLID, a model in one-dimensional space is useful [20]. In this paper, however, rather than consider general  $nD$  space, we restrict discussion to  $n=3$  for ease of presentation.

It is important to bear in mind that, throughout this paper, we use the notation that subscript  $k$  stands for  $g, e, s, d$  (Appendix A), while subscript  $j$  stands for  $g, e$ . The respective distribution functions of velocity  $\mathbf{v}$  at time  $t$  are denoted by  $f_j(\mathbf{v}; t)$ , and are normalized so that the concentrations, denoted by  $c_j(t)$ , which satisfy

$$c_s(t) = c_g(t) + c_e(t) = 1, \quad (2.1)$$

are given (Appendix A) by

$$c_k(t) = I_{1k}(t). \quad (2.2)$$

Our (FP) geometry is that used in most theoretical work to date; that is, we consider initially free-molecule flow across an open cell lying between two equilibrium reservoirs with molecular number-density difference  $\Delta\rho=0$  and pressure difference  $\Delta P=0$ . LID results in a gas flow across the cell, which is balanced in a closed cell by the existence of non-zero  $\Delta\rho$  and  $\Delta P$  (the latter of which is measured experimentally). The flow is between parallel plates oriented normal to the  $z$  axis. The laser beam runs in the  $x$  direction, and the sides of the rectangular parallelepiped (that is, the cell) containing the gas are  $X, Y, Z$  in an obvious notation (for example, it is the ratio  $Z/X$  which would be made small to enhance the SLID effect). Implicit in the model is that the limits of large  $X$  and large  $Y$  are understood, that is, there are no side effects or end effects.

The SLID effects originate in the collisions of the gas molecules with the (active) surfaces (walls), that is, those oriented normal to the  $z$  axis. In order to have a BLID effect, buffer particles are assumed to be present in the gas and are assumed for simplicity to be of effectively infinite mass. When a gas molecule collides with a surface or with a buffer particle, it is assumed to be scattered into the gas according to a Maxwellian accommodation coefficient model. When scattering from a surface, fractions  $\alpha_{s,j}$  enter diffuse velocity distributions, while the remaining fractions  $(1 - \alpha_{s,j})$  are scattered ‘‘specularly,’’ which means that their  $z$  components of velocity,  $v_z$ , change sign; when scattering from a buffer particle, fractions  $\alpha_{b,j}$  enter (different) diffuse velocity distributions, while the remaining fractions  $(1 - \alpha_{b,j})$  are scattered ‘‘specularly,’’ which means in this case that they undergo no change of velocity. The fraction of diffuse-scattering collisions of the atoms with the surfaces, which results in quenching from excited state to ground state, is denoted by  $z_s$ , and the analogous quantity for collisions with the buffer particles by  $z_b$ . In fact, the description of molecule-particle scattering in terms of molecule-particle accommodation coefficients  $\alpha_{b,j}$  is on far shakier ground than that of molecule-surface scattering in terms of molecule-surface accommodation coefficients  $\alpha_{s,j}$ , and needs further attention and discussion. Similar remarks apply to the use of the quenching fractions  $z_b$  and  $z_s$ , and we hope to address these issues in future publications.

The laser excitation is modeled as in previous work, that is, via an excitation-frequency function  $q(v_x)$  given by

$$q(v_x) = \int d\omega \frac{\Theta \lambda(\omega) \Gamma / \pi}{\Gamma^2 + (\omega - \omega_0 - kv_x)^2}, \quad (2.3)$$

where  $\Theta$  is an Einstein coefficient,  $\lambda(\omega)d\omega$  is the laser radiation energy density in the radiation frequency interval  $d\omega$  at  $\omega$ ,  $\omega_0$  is the resonant frequency,  $\Gamma$  is the absorption half line width at half maximum [11], and where the laser radiation wave-number vector  $\mathbf{k} = (k, 0, 0)$ .

Provided that a reasonable representation of the function  $q(v_x)$  is available, there is in fact no need to parametrize it

further. However, it is convenient [8] to do so using the Heaviside step function, which we denote by  $h$ , as follows:

$$q(v_x) = q_0[h(v_x - v_a) - h(v_x - v_b)], \quad (2.4)$$

where  $v_a < v_b$ , letting  $q(v_x)$  operate in the interval  $v_a < v_x < v_b$  with constant value  $q_0$ , where either or both of  $-v_a$  and  $v_b$  could be  $\infty$ ; for example, Ref. [8] uses Eq. (2.4) with  $v_a = 0$ ,  $v_b = \infty$ .

Again as in previous work, a decay parameter  $\gamma$  is introduced to model the effective spontaneous quenching of excited molecules. With the definitions made so far, we may build the MBREs. In doing so, we need the frequencies of collisions of the molecules with the surfaces and with the buffer particles. For the surfaces for molecules of velocity  $\mathbf{v}$ , the frequency is  $|v_z|/Z$ ; the average frequencies are  $\langle |v_z| \rangle_j / Z$  where, more generally,  $\langle \xi \rangle_k(t)$  stands for [21] the results of averaging  $\xi(\mathbf{v}; t)$  with respect to  $\mathbf{v}$  over  $f_k(\mathbf{v}; t)$ , that is, in terms of the concentrations  $c_k$ , Eq. (2.2),

$$c_k(t) \langle \xi \rangle_k(t) = \int \int \int d^3 \mathbf{v} \xi(\mathbf{v}; t) f_k(\mathbf{v}; t). \quad (2.5)$$

For the buffer particles, again for molecules of velocity  $\mathbf{v}$ , the frequency is  $\theta v$ , where  $\theta$  is an inverse mean free path, defined as the average of the inverse path lengths experienced by a gas molecule between collisions; the average frequencies are  $\langle \theta v \rangle_j$ .

Before proceeding, let us make clear the parameters of the model. With the excitation-frequency function  $q(v_x)$  parametrized according to Eq. (2.4), there are the 11 parameters  $q_0$ ,  $v_{a,b}$ ,  $\alpha_{sj}$ ,  $\alpha_{bj}$ ,  $z_{s,b}$ ,  $\gamma$  and  $\theta$ . For the purposes of this paper, we assume that none of these parameters depends on  $\mathbf{v}$ ; in the author's opinion, it makes little sense to assume otherwise in a model of this type.

We now proceed to dimensionless quantities. Readers are asked to pretend that every dimensional quantity appearing above has an asterisk attached, for example,  $Z^*$  and  $f_k^*(\mathbf{v}^*; t^*)$ . Characteristic dimensional quantities (energy  $E_c^*$ , length  $l_c^*$ , temperature  $T_c^*$ , speed  $v_c^*$ ) are chosen to give our dimensionless quantities, which will have no asterisks; our choice gives

$$\hbar \omega = Z = b = 2T/\mu = 1, \quad (2.6)$$

where  $b^*$  is the Boltzmann constant,  $T^*$  is the temperature,  $\mu^*$  is the gas molecular mass, and  $2\pi\hbar^*$  is Planck's constant. From this point on, unless otherwise made clear, the analysis is presented in terms of the resulting dimensionless quantities.

With the parameter definitions made above, our MBREs are [22]

$$\begin{aligned} \partial f_g / \partial t = & (c_g \alpha_{sg} \langle |v_z| \rangle_g + c_e \alpha_{se} z_s \langle |v_z| \rangle_e) M + (c_g \alpha_{bg} \langle v \rangle_g \\ & + c_e \alpha_{be} z_b \langle v \rangle_e) \theta B - (\alpha_{sg} |v_z| + \alpha_{bg} \theta v) f_g + \gamma f_e \\ & - q(f_g - f_e), \end{aligned} \quad (2.7a)$$

$$\begin{aligned} \partial f_e / \partial t = & c_e \alpha_{se} (1 - z_s) \langle |v_z| \rangle_e M + c_e \alpha_{be} (1 - z_b) \theta \langle v \rangle_e B \\ & - (\alpha_{se} |v_z| + \alpha_{be} \theta v + \gamma) f_e + q(f_g - f_e), \end{aligned} \quad (2.7b)$$

where  $M(\mathbf{v})$  and  $B(\mathbf{v})$  are appropriate velocity distribution functions (Appendix B). It is important to note that they are not the bulk-Maxwellian distribution  $m(\mathbf{v})$ : for example, a gas molecule undergoing diffuse scattering at a surface chooses its velocity based on the distribution  $M(\mathbf{v})$ , and not on  $m(\mathbf{v})$ . It is easy to see that using  $m$  instead of  $M$  and  $B$  is wrong: for example, with  $\alpha_{bj} = \gamma = q = 0$ , it follows from Eq. (2.7) with  $\partial f_j / \partial t = 0$  that

$$f_j^{(ss)} = c_j^{(ss)} \langle |v_z| \rangle_j M / |v_z| = (1, 0) m, \quad (2.8a)$$

where superscript  $(ss)$  denotes the steady state throughout this paper, and this result is correct; also, with  $\alpha_{sj} = \gamma = q = 0$ , we get the same correct result, this time via

$$f_j^{(ss)} = c_j^{(ss)} \langle v \rangle_j B / v = (1, 0) m. \quad (2.8b)$$

Much previous work is not quite right at this point. For example, if we put  $a_j = 1$ ,  $\alpha_j = \gamma = Q = 0$  in Eqs. (1) and (2) of Ref. [11], we get the incorrect results  $f_j^{(ss)} = c_j \langle |v_z| \rangle_j m / |v_z|$ , and we expand on this point below.

We now eliminate  $M$  and  $B$  from Eq. (2.7) in favor of  $m$ , using Appendix B. On defining  $\beta_{zj}$  and  $\beta_{vj}$  from

$$\langle |v_z| \rangle_m \beta_{zj} = \langle |v_z| \rangle_j, \quad (2.9a)$$

$$\langle v \rangle_m \beta_{vj} = \langle v \rangle_j, \quad (2.9b)$$

the MBREs (2.7) may be written as

$$\begin{aligned} \partial f_g / \partial t = & [(c_g \alpha_{sg} \beta_{zg} + c_e \alpha_{se} z_s \beta_{ze}) |v_z| + (c_g \alpha_{bg} \beta_{vg} \\ & + c_e \alpha_{be} z_b \beta_{ve}) \theta v] m - (\alpha_{sg} |v_z| + \alpha_{bg} \theta v) f_g + \gamma f_e \\ & - q(f_g - f_e), \end{aligned} \quad (2.10a)$$

$$\begin{aligned} \partial f_e / \partial t = & [c_e \alpha_{se} (1 - z_s) \beta_{ze} |v_z| + c_e \alpha_{be} (1 - z_b) \beta_{ve} \theta v] m \\ & - (\alpha_{se} |v_z| + \alpha_{be} \theta v + \gamma) f_e + q(f_g - f_e). \end{aligned} \quad (2.10b)$$

In terms of the integrals in Appendix A, the  $\beta$ 's are given by

$$\beta_{zj}(t) = \pi^{1/2} I_{zj}(t) / I_{1j}(t), \quad (2.11a)$$

$$\beta_{vj}(t) = \frac{1}{2} \pi^{1/2} I_{vj}(t) / I_{1j}(t). \quad (2.11b)$$

The assumptions which have been made by most of the previous work, and which are not quite right, are precisely

$$\beta_{zj}(t) = \beta_{vj}(t) = 1, \quad (2.12)$$

and are in fact good approximations in that work because the distributions therein are close to Maxwellian because of the assumed small radiation intensities. The assumption made in Ref. [11] is somewhat different, however, involving effectively the equating of  $|v_z|$  to  $\langle |v_z| \rangle_m$ .

Interest so far has always been in approximate steady-state solutions, which have been found by setting  $\partial f_j / \partial t = 0$  and making subsequent approximations. Although we

are about to embark on obtaining exact solutions, it must always be borne in mind that use of the parametrized function  $q(v_x)$ , and of the eight remaining parameters, is a gross approximation in itself.

Some discussion on how to get model equations for pure SLID and pure BLID from Eq. (2.10) is in order. At first sight, it may seem that the appropriate molecular collision frequency should be set equal to zero ( $\theta v = 0$  for pure SLID and  $|v_z| = 0$  for pure BLID). However, for pure SLID, it is strictly only necessary that  $\alpha_{bg} = \alpha_{be}$ , and, for pure BLID, that  $\alpha_{sg} = \alpha_{se}$ . However, neither of these equalities leads to significant simplification at the stage of Eq. (2.10). For pure SLID, the suggestion (setting  $\theta v = 0$ ) made above is reasonable on the grounds that this assumes that the mean free paths are large, when BLID will be negligible. For pure BLID, however, setting  $|v_z| = 0$  is perhaps not as sensible, because this neglects surface effects which will be present even in the absence of SLID (when  $\alpha_{sg} = \alpha_{se}$ ); however, setting  $|v_z| = 0$  does give a reasonable model of pure BLID, and is perhaps the cleanest way of getting one. When we specialize to pure SLID here, we put  $\theta v = 0$ ; we do not specialize to pure BLID here.

### III. RELATIONSHIP WITH EXPERIMENTAL MEASUREMENTS

Explicit time dependences are omitted for the moment, as are the superscripts (*ss*), since the main interest has been in steady-state measurements. The quantities of greatest interest are the so-called ‘‘LID fluxes,’’ which are defined as the integrals of  $v_x$  over the distributions  $f_k$  and are given by  $I_{xk}$  (Appendix A). The flux sum  $I_{xs}$  may be related to potential experimental quantities such as the resulting pressure difference  $\Delta P = X dP/dx$  across the cell, the laser radiation power intensity absorbed by the gas denoted by  $r$  ( $r^*$  has dimensions power/area), and the concentration  $c_e$  of excited molecules, given by Eq. (2.2).

The relation between  $\Delta P$  and  $I_{xs}$  is

$$\Delta P = \kappa X P I_{xs}, \quad (3.1)$$

where  $\kappa$  is a constant, which in real applications will be of order unity, and which depends on the actual system being modeled, with  $P$  on the right-hand side (RHS) of Eq. (3.1) standing for the average active-gas (partial) pressure in the cell; the choice of  $\kappa$  is discussed further in Sec. VI.

It follows from Eq. (2.10) that the contribution to  $\partial f_e / \partial t$  from the radiation is  $q(f_g - f_e)$ , from which we deduce, by integration over  $\mathbf{v}$ , that the laser contribution to  $dN_e/dt$ , where  $N_e$  is the number of excited molecules from a total of  $N$ , is given by

$$(dN_e/dt)_{\text{laser}} = N I_{qd}. \quad (3.2)$$

It takes unit energy [22] to excite one molecule, so that the absorbed radiation intensity is given by [22]  $Y^{-1}(dN_e/dt)_{\text{laser}}$ , which gives

$$r = \rho X I_{qd}. \quad (3.3)$$

We may combine the above results to get several formulas which are candidates for comparison with experiment. To this end, we define the quantity  $\delta$  by

$$\delta = (\Delta P/P)/(r/\rho) \quad (3.4)$$

for use below, particularly in Sec. VI; for example, Eqs. (2.2), (3.1), (3.3), and (3.4) give

$$\delta = \kappa I_{xs}/I_{qd}, \quad (3.5)$$

$$c_e/(r/\rho) = X^{-1} I_{1e}/I_{qd}. \quad (3.6)$$

It is sometimes useful, particularly when comparison with experiment is contemplated, to express results in terms of dimensional (asterisked) quantities. To this end, we introduce ‘‘standard quantities,’’ based on experiment [14,16]. Using the perfect gas law to eliminate  $\rho$ , we may write Eqs. (3.3) and (3.5) as follows:

$$\left(\frac{r^* \text{ mm}^2}{\text{mW}}\right) \approx 196 \left(\frac{X^*/10 \text{ cm}}{Z^*/\text{mm}}\right) \left(\frac{P^*}{\text{Pa}}\right) \times \left(\frac{30 \text{ amu}}{\mu^*}\right)^{1/2} \left(\frac{300 \text{ K}}{T^*}\right)^{1/2} \left(\frac{10 \text{ }\mu\text{m}}{\lambda^*}\right) I_{qd}, \quad (3.7)$$

$$\frac{(\Delta P^*/\text{m Pa})}{(r^* \text{ mm}^2/\text{mW})} \approx 511 \kappa \left(\frac{\mu^*}{30 \text{ amu}}\right)^{1/2} \left(\frac{T^*}{300 \text{ K}}\right)^{1/2} \left(\frac{\lambda^*}{10 \text{ }\mu\text{m}}\right) \frac{I_{xs}}{I_{qd}}, \quad (3.8)$$

where amu is the atomic mass unit ( $\approx 1.7 \times 10^{-27}$  kg) and  $\lambda^*$  is the radiation wavelength; our choice of standard quantities is clear from Eqs. (3.7) and (5.15) and the last sentence of Appendix H.

With other theoretical parameters fixed, Eq. (3.7) allows the calculation of  $q_0$ , via  $I_{qd}$ , from experimental data. As expected,  $q_0$  and  $I_{qd}$  may be of the same order, implying that small  $q_0$  gives an important special case for us. Contact between theory and experiment is based on Eqs. (2.2), (3.7), and (3.8), thus highlighting the importance of the three integrals  $I_{1e}$ ,  $I_{xs}$ , and  $I_{qd}$ .

Finally, it must be borne in mind that the experiments are not done with our idealized geometry; actual values [14,16] of  $X$  and  $Y$  are not very large, although  $X$  is reasonably large; we make no attempt in the theory to account for the fact that  $X$  and  $Y$  may not be very large, with the hope that reasonable comparisons may still be made.

## IV. NUMERICAL SOLUTION OF THE RATE EQUATIONS

### A. Iteration of the analytical steady-state equations

The author’s opinion is that the most interesting and illuminating way to solve the MBREs (2.10) is by numerical integration with respect to time  $t$ , although this is a relatively time-consuming procedure. We delay discussion of this procedure (Section IV B) until the iteration solution has been described.

The conditions  $\partial f_j / \partial t = 0$  enable Eq. (2.10) to be solved for  $f_j^{(ss)}$  in terms of the (unknown as yet)  $c_j^{(ss)}, \beta_{zj}^{(ss)}, \beta_{vj}^{(ss)}$ . We drop the superscripts  $(ss)$  for now. We write

$$f_j(\mathbf{v}) = f_j^{(\text{num})} / f_j^{(\text{den})} \quad (4.1)$$

in an obvious notation. It is useful to define the following collections of terms:

$$t_{oj} = \alpha_{sj} |v_z| + \alpha_{bj} \theta v, \quad (4.2a)$$

$$t_{\beta j} = \alpha_{sj} \beta_{zj} |v_z| + \alpha_{bj} \beta_{vj} \theta v, \quad (4.2b)$$

$$t_e = \alpha_{se} z_s \beta_{ze} |v_z| + \alpha_{be} z_b \beta_{ve} \theta v, \quad (4.2c)$$

when  $f_j^{(\text{num})}$  and  $f_j^{(\text{den})}$  are given from the following relations:

$$f_g^{(\text{num})} / m = (c_g t_{\beta g} + c_e t_e) t_{og} + (c_g t_{\beta g} + c_e t_{\beta e})(q + \gamma), \quad (4.3a)$$

$$f_e^{(\text{num})} / m = c_e (t_{\beta e} - t_e) t_{og} + (c_g t_{\beta g} + c_e t_{\beta e}) q, \quad (4.3b)$$

$$f_j^{(\text{den})} = (t_{oe} + \gamma) t_{og} + (t_{og} + t_{oe}) q. \quad (4.3c)$$

The solution proceeds as follows. Values of  $c_j, \beta_{zj}, \beta_{vj}$  are chosen, say, as follows:

$$c_g = 1, \quad c_e = 0, \quad \beta_{zj} = \beta_{vj} = 1. \quad (4.4)$$

The distributions  $f_j$  are calculated from Eqs. (4.1)–(4.3), and the five integrals  $I_{1g}, I_{zj}, I_{vj}$  (Appendix A) are computed. More accurate values of  $c_g, \beta_{zj}, \beta_{vj}$  may now be calculated using Eqs. (2.2) and (2.11), and then that of  $c_e$  using Eq. (2.1). Updated versions of  $f_j$  are now calculated, and the iteration process proceeds in the obvious way until convergence to the desired accuracy is attained. It must be noted that, during the iteration, the more accurate values of both  $c_j$ 's must not be calculated from Eq. (2.2), or else the iteration will converge to a solution which does not satisfy Eq. (2.1); naturally, the more accurate value of  $c_e$  rather than of  $c_g$  could be calculated from Eq. (2.2), and then that of  $c_g$  from Eq. (2.1).

Computations to several-digit accuracy (entirely unnecessary, of course) typically involve of the order of tens of iterations, although many more are sometimes necessary, particularly for small  $q_0$ , but with each case taking less than a second of computer time. All steady-state properties are now readily computed, as with the (hopefully the same) solution from Sec. IV B.

### B. Integration of the MBREs with respect to time

The MBREs (2.10) are integrated with respect to time  $t$ , from an initial value ( $t=0$ ) to a final value ( $t=t_f$ ) at which convergence to a desired accuracy is attained; observing the distributions relax from their initial conditions to their steady states is most enjoyable. Initial conditions are trivially chosen, for example,

$$f_g(\mathbf{v}; 0) = m(\mathbf{v}), \quad f_e(\mathbf{v}; 0) = 0, \quad (4.5)$$

implying that  $c_g(0) = 1 - c_e(0) = 1$ , and the infinitude of possible choices yields excellent checks.

This integration procedure is naturally relatively time consuming: at each time step in the computation,  $c_j$  must be computed using Eqs. (2.1) and (2.2), as well as  $\beta_{zj}$  and  $\beta_{vj}$  using Eq. (2.11), involving integrations with respect to  $\mathbf{v}$  of  $1, |v_z|$ , and  $v$  over both of  $f_j$  [23]. [Both integrations of 1 should be done in order to use Eqs. (2.1) and (2.2) to check the computation.] Once convergence is attained at  $t=t_f$ , we put

$$f_j^{(ss)}(\mathbf{v}) = f_j(\mathbf{v}; t_f), \quad (4.6)$$

after which all steady-state properties are again readily computed, the results from Sec. IV A above forming obvious checks.

In the computations, particularly because the  $f_j^{(ss)}(\mathbf{v})$  are close to (perhaps piecewise) Maxwellian distributions in important cases, it is helpful to work with new velocity variables  $s_l$  having ranges  $-1 < s_l < 1$  and for which the Maxwellian distribution  $m(\mathbf{s})$  is constant in these ranges: such variables are uniquely defined by

$$s_l = \text{erf} v_l, \quad (4.7)$$

when, in 3D space,

$$m(\mathbf{s}) = \frac{1}{8} : -1 < s_l < 1. \quad (4.8)$$

The author's computations use the simplest step wise numerical integration with respect to  $t$ , with  $t_f$  and  $\Delta t$  chosen by trial and error; the integrations with respect to  $\mathbf{s}$  use step sizes  $\Delta s_l$ , again found by trial and error.

Typically,  $\Delta s_l \sim 0.05$  is chosen, but choices of  $t_f$  and  $\Delta t$  depend strongly on the case considered. Although trial and error is easily the best procedure, some rough indications of suitable values of  $t_f$  and  $\Delta t$  may be gleaned from the consideration of a relaxation time  $\tau$  for the process. Definition of  $\tau$  is somewhat arbitrary, but it is shown in Appendix C that one reasonable choice gives

$$\tau^{-1} \sim \pi^{-1/2} (\alpha_{se} z_s + 2 \alpha_{be} z_b \theta) + \gamma + q_0 d(\text{erf}), \quad (4.9)$$

with  $d(\text{erf})$  defined by

$$d(\text{erf}) = \text{erf} v_b - \text{erf} v_a. \quad (4.10)$$

One may start the trial-and-error procedure by trying, say,  $t_f = 100\tau$  and  $\Delta t = \tau/100$ , making  $t_f/\Delta t$  (the number of time-integration steps) as small as possible for the given desired accuracy. To compare nicely with the relatively very fast and accurate computations described in Sec. IV A, several-digit accuracy may require values of  $t_f$  considerably larger and/or values of  $\Delta t$  considerable smaller than the simple estimates made above.

A typical computation on the SIG dual-tower Origin 2000 machine (with four 270-MHz R 12000 processors) called SCIENIDE at Waterloo, for a 2D model of BLID/SLID, takes of the order of minutes. Computations with a 3D model (unnecessary for pure SLID) have not yet been done, but,

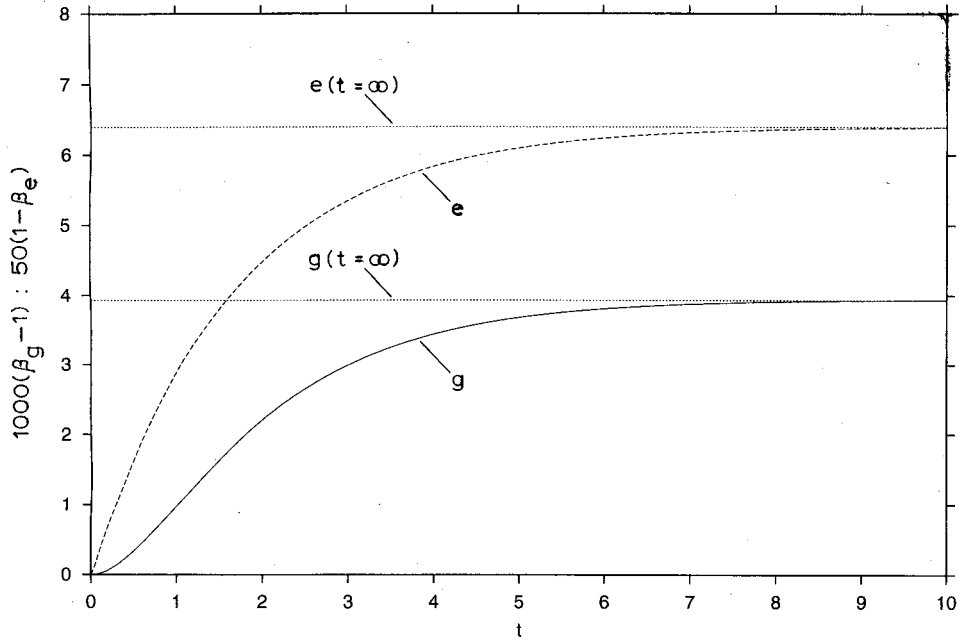


FIG. 1. Time dependence of the  $\beta_j$  for a case of pure SLID: the initial conditions are Eqs. (4.5), with  $\alpha_g=0.99$ ,  $\alpha_e=0.98$ ,  $z_s=0.5$ ,  $\gamma=0.5$ ,  $q_0=0.05$ ,  $v_a=0$ ,  $v_b=\infty$ , giving relaxation time  $\tau \approx 1.21$ . The curve (—) is related to  $\beta_g$  and (---) to  $\beta_e$ ; the horizontal lines (·····) give the steady-state values, which are  $\beta_g \approx 1.00393$  and  $\beta_e \approx 0.872$ .

with  $\Delta s_k$  still of order 0.05, each may take of the order of an hour on the same machine. It must be emphasized that these computation times of minutes or hours are totally unnecessary if only accurate steady-state results are required (Sec. IV A).

The author regards his computations where BLID is involved as incomplete, and results are presented here only for pure SLID ( $\theta v=0$ ). As an example, we show in Fig. 1 the time dependence of the  $\beta_j$  (the subscripts  $z$  may be dropped here) with initial conditions (4.5); the parameters are listed in the caption, and  $\tau \approx 1.21$  from Eq. (4.9). The steady-state values are  $\beta_g \approx 1.00393$ ,  $\beta_e \approx 0.872$ , which illustrates that the assumptions (2.12) made by others are reasonable; the  $\beta_j$  are close to unity because the distributions  $f_j$  are close to Maxwellian, echoing the remarks made above concerning the definition (4.7).

## V. EXACT ANALYTICAL STEADY-STATE SOLUTION FOR SLID

### A. The general case

With  $\theta v=0$ , and  $z$ ,  $\alpha_j$ ,  $\beta_j$  standing for  $z_s$ ,  $\alpha_{sj}$ ,  $\beta_{zj}$ , it follows from Eqs. (4.1)–(4.3) that the  $f_j$  are given from

$$\frac{f_j}{m} = \frac{A_j |v_z| + Bq(v_x) + \gamma E_j}{C|v_z| + Dq(v_x) + \gamma F}, \quad (5.1)$$

with the eight constants defined by

$$A_g = (c_g \alpha_g \beta_g + c_e \alpha_e z \beta_e) \alpha_e, \quad (5.2a)$$

$$A_e = c_e \alpha_g \alpha_e (1-z) \beta_e, \quad (5.2b)$$

$$B = c_g \alpha_g \beta_g + c_e \alpha_e \beta_e, \quad (5.2c)$$

$$C = \alpha_g \alpha_e, \quad (5.2d)$$

$$D = \alpha_g + \alpha_e, \quad (5.2e)$$

$$E_g = B, \quad (5.2f)$$

$$E_e = 0, \quad (5.2g)$$

$$F = \alpha_g. \quad (5.2h)$$

In order to proceed, we need to do the eight integrals (Appendix A)  $I_{1j}$ ,  $I_{xj}$ ,  $I_{zj}$ , and  $I_{qj}$ . With the function  $G(u)$  defined as in Appendix D, the required integrals may be done in closed form and are presented in Appendix E, in which an analog,  $d(\exp)$ , of  $d(\text{erf})$ , Eq. (4.10), is defined [Eq. (E4)].

Everything is still expressed in terms of the four as yet unknowns  $c_j$  and  $\beta_j$ , and these are found by solving the system of four equations

$$c_j = I_{1j}, \quad (5.3a)$$

$$c_e + c_g = 1, \quad (5.3b)$$

$$c_e \beta_e = \pi^{1/2} I_{ze}, \quad (5.3c)$$

where Eq. (5.3c) could have subscripts  $e$  replaced by  $g$ , giving a check. The solution may now be completed, and the important results for  $I_{1e}$ ,  $I_{qd}$  and  $I_{xs}$  are given in Appendix F.

Next, we study some simple special cases, motivated by previous work. Bearing in mind Eqs. (E2) and (E3), our spe-

cial cases involve the limit of small  $a$ , with perhaps  $g=0$ ,  $z>0$ , or  $z=0$ ,  $g>0$  [24]. Great care is required when studying these special cases, an origin of which is the noncommutation of the two limits  $a\rightarrow 0$ ,  $g\rightarrow 0$ , as is made clear by the exact result

$$\lim_{a\rightarrow 0} \left( \frac{-1}{a \ln a} \lim_{g\rightarrow 0} G_w \right) = \lim_{g\rightarrow 0} \left( \frac{-1}{g \ln g} \lim_{a\rightarrow 0} G_w \right) = \frac{2}{\pi^{1/2}}, \quad (5.4)$$

where readers are reminded of the definition (E6) of  $w$ . This means, for example, that if we are interested in the case  $a\rightarrow 0$  with  $a/g \gg 1$  (including the case  $g=0$ ), then we should set  $g=0$  first and then let  $a\rightarrow 0$ ; for the case  $a\rightarrow 0$  with  $a/g \ll 1$ , we should let  $a\rightarrow 0$  in the general case. The case  $a\rightarrow 0$  with  $a$  of the same order as  $g$  is not likely to be of interest and will be ignored. There is no problem in the case  $a\rightarrow 0$  for any value of  $z$  because the limits  $a\rightarrow 0$ ,  $z\rightarrow 0$  commute.

The special case (a) is the limit of small  $a$  in the general case ( $g>0$ ,  $z>0$ ). Case (b) has  $g=0$ ,  $z>0$ , and case (b') involves the limit of small  $a$  in case (b) [8]; case (c) has  $z=0$ ,  $g>0$ , and case (c') involves the limit of small  $a$  in case (c) [3–7,9–11].

## B. Special cases

### 1. Case (a): $a\rightarrow 0$ in the general case

The three important integrals are as follows:

$$\frac{I_{1e}}{a} \rightarrow \frac{(zG_g + ygH_g)}{g(z + ygH_g)} \frac{\alpha_g}{\Sigma\alpha} \frac{d(\text{erf})}{2}, \quad (5.5a)$$

$$\frac{I_{xs}}{a} \rightarrow \frac{G_g}{\pi^{1/2}g} \frac{\Delta\alpha}{\Sigma\alpha} \frac{d(\text{exp})}{2}, \quad (5.5b)$$

$$\frac{I_{qd}}{a} \rightarrow \frac{\alpha_g\alpha_e}{\Sigma\alpha} \frac{d(\text{erf})}{2}. \quad (5.5c)$$

One may manipulate the results in many ways. For example, the work of Sec. III motivates us to write

$$\delta \rightarrow \frac{\kappa}{\pi^{1/2}} \frac{G_g}{g} \frac{d(\text{exp})}{d(\text{erf})} \frac{\Delta\alpha}{\alpha_g\alpha_e}. \quad (5.6)$$

If  $v_b \approx v_a$ , when  $(v_b + v_a)$  is customarily [14,15] denoted by  $2v_L$ , then we may write, in an obvious notation, a prescription for expressing our results in terms of  $v_L$ , that is,

$$\frac{d(\text{exp})}{d(\text{erf})} \rightarrow \frac{2ve^{-v^2}dv}{2e^{-v^2}dv/\pi^{1/2}} = \pi^{1/2}v_L, \quad (5.7)$$

giving

$$\delta \rightarrow \kappa v_L \frac{G_g}{g} \frac{\Delta\alpha}{\alpha_g\alpha_e}. \quad (5.8)$$

### 2. Case (b): $g=0$ with $z>0$

The results are given in Appendix G. We pass on to the important case (b'), which is the case studied in Ref. [8].

### 3. Case (b'): Case (b) with small $a$

The three important integrals are, including only the necessary leading terms, Eq. (5.5c) and

$$\frac{I_{1e}}{a} \rightarrow \left[ -\ln a - \frac{\sigma}{2} + \frac{\pi^{1/2}y}{2z} \right] \frac{\alpha_g}{\Sigma\alpha} \frac{d(\text{erf})}{\pi^{1/2}}, \quad (5.9a)$$

$$\frac{I_{xs}}{a} \rightarrow \left[ -\ln a - \frac{\sigma}{2} \right] \frac{\Delta\alpha}{\Sigma\alpha} \frac{d(\text{exp})}{\pi}. \quad (5.9b)$$

Unless  $a$  is very small, and perhaps outside of experimental accessibility, the terms in square brackets in Eq. (5.9) should all be kept, at least at first; for example, for  $-\ln a$  to dominate in Eq. (5.9a) with  $z=0.5$ ,  $a$  must be less than about  $10^{-5}$ . We obtain (Sec. III), in particular for comparison with the work of Ref. [8], the following results:

$$\frac{-\delta}{(\ln a + \sigma/2)} \rightarrow \frac{2\kappa}{\pi} \frac{\Delta\alpha}{\alpha_g\alpha_e} \frac{d(\text{exp})}{d(\text{erf})}, \quad (5.10a)$$

$$\frac{-c_e}{(\ln a + \sigma/2 - \pi^{1/2}y/2z)r/\rho} \rightarrow \frac{2}{\pi^{1/2}X\alpha_e}, \quad (5.10b)$$

$$a \rightarrow \frac{r\Sigma\alpha}{\rho X\alpha_g\alpha_e} \frac{2}{d(\text{erf})}. \quad (5.10c)$$

To compare with Ref. [8] we see, from their Eq. (15) and our Eq. (3.1), that they effectively interpret our  $\kappa$  via  $\kappa = 1/v_T$ . They have  $d(\text{exp})=d(\text{erf})=1$ , and so their Eq. (17) reads as our Eq. (5.10a), but with an additional factor  $[-(\ln a + \sigma/2)\ln X/X]$  multiplying the RHS. We believe Eq. (5.10a) to be exact (for  $g=0$  and small  $a$ ), so we conclude that those differences are an artifact of their approximations.

It is interesting that, in the case (b'), both  $\Delta P/r$  and  $c_e/r$  are proportional, for small  $r$ , to  $-\ln a$  rather than being constant. This prediction may be testable experimentally, and so we present Eq. (5.10) in terms of our standard quantities (Sec. III):

$$\begin{aligned} & \frac{-(\Delta P^*/\text{mPa})}{(\ln a + \sigma/2)(r^*\text{mm}^2/\text{mW})} \\ & \approx 326\kappa \frac{d(\text{exp})}{d(\text{erf})} \frac{\Delta\alpha}{\alpha_g\alpha_e} \\ & \times \left( \frac{\mu^*}{30 \text{ amu}} \right)^{1/2} \left( \frac{T^*}{300 \text{ K}} \right)^{1/2} \left( \frac{\lambda^*}{10 \text{ }\mu\text{m}} \right), \quad (5.11a) \end{aligned}$$

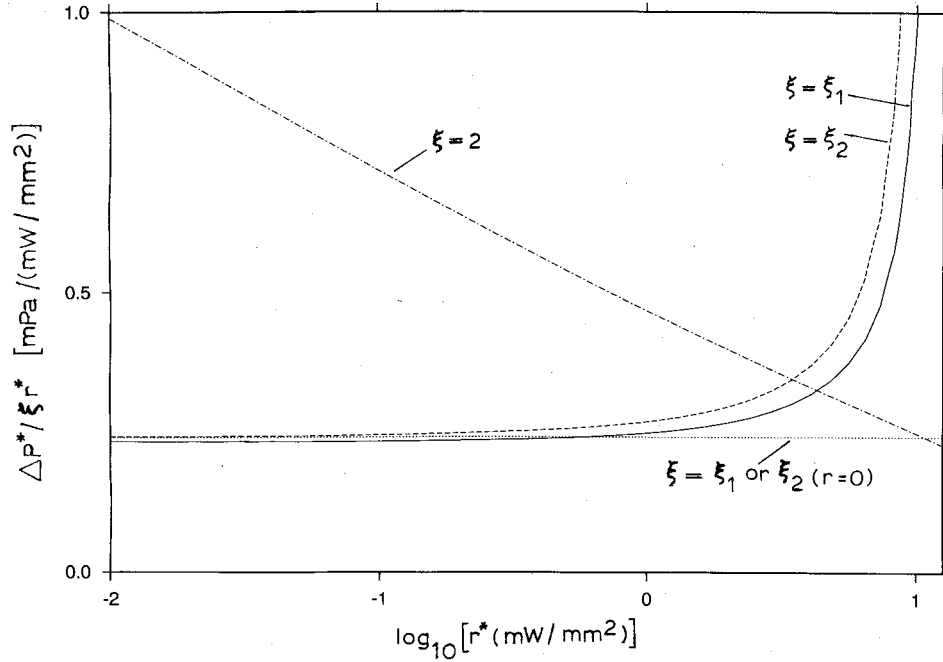


FIG. 2. Dependence on  $r$  of  $\Delta P/\xi r$  for [21]  $\xi=2$  (---),  $\xi=\xi_1=-\ln a$  (—), and  $\xi=\xi_2=-\ln a-\sigma/2$  (- · - · -); the horizontal line (·····) gives the limit as  $r\rightarrow 0$ , with either  $\xi=\xi_1$  or  $\xi=\xi_2$ , which is about 0.240. The parameters are  $\alpha_g=1$ ,  $\alpha_e=0.999$ ,  $z=0.5$ ,  $\gamma=0$ ,  $v_a=0$ ,  $v_b=\infty$ , with  $a$  varying as necessary to produce the results.

$$\frac{-1000c_e/(r^*\text{mm}^2/\text{mW})}{(\ln a + \sigma/2 - \pi^{1/2}y/2z)} \approx \frac{5.77}{\alpha_e} \left( \frac{\text{Pa}}{P^*} \right) \left( \frac{Z^*/\text{mm}}{X^*/10 \text{ cm}} \right) \times \left( \frac{\mu^*}{30 \text{ amu}} \right)^{1/2} \left( \frac{T^*}{300 \text{ K}} \right)^{1/2} \left( \frac{\lambda^*}{10 \text{ }\mu\text{m}} \right), \quad (5.11b)$$

$$100a \approx \left( \frac{1.023\Sigma\alpha}{\alpha_g\alpha_e d(\text{erf})} \right) \left( \frac{r^*\text{mm}^2}{\text{mW}} \right) \left( \frac{Z^*/\text{mm}}{X^*/10 \text{ cm}} \right) \left( \frac{\text{Pa}}{P^*} \right) \times \left( \frac{\mu^*}{30 \text{ amu}} \right)^{1/2} \left( \frac{T^*}{300 \text{ K}} \right)^{1/2} \left( \frac{\lambda^*}{10 \text{ }\mu\text{m}} \right). \quad (5.11c)$$

The situation is perhaps clarified by considering a special case in Fig. 2, using the parameters listed in the caption. With our standard quantities (excluding  $\Delta P^*$  and  $r^*$ ), we show exact results for  $(\Delta P/\xi r)$  as functions of  $r$  for three values of  $\xi$  [21]:  $\xi=2$  gives a usual  $(\Delta P/r)$  versus  $r$  plot;  $\xi=\xi_1=-\ln a$  is a more sensible choice for very small  $a$  (and hence of  $r$ ), but  $\xi=\xi_2=-\ln a+\sigma/2$  is preferable here because of the form of Eq. (5.11a) and the fact that  $a$  is not small enough for  $\xi=\xi_1$  to be adequate [it is clear from Eq. (5.11c) that realistic values of  $a$  are of order  $10^{-2}$ , the values for Fig. 4 ranging from about  $2 \times 10^{-4}$  to about 0.6, whereas  $a < \text{about } 10^{-5}$  for  $\xi_1$  to be adequate, as discussed above].

#### 4. Case (c): $z=0$ with $g>0$

For this case, a little thought leads to the conclusion that we must have

$$r = \rho X g \alpha_e c_e, \quad I_{qd} = g \alpha_e I_{1e}, \quad (5.12)$$

which form good checks on the computations. Apart from Eq. (5.12), this case does not lead to as great a simplification as does case (b), and we may as well use the general case directly.

#### 5. Case (c'): Case (c) with small $a$

We get Eqs. (5.5b) and (5.5c) with (5.5a) becoming

$$\frac{I_{1e}}{a} \rightarrow \frac{\alpha_g}{\Sigma\alpha} \frac{d(\text{erf})}{2g}, \quad (5.13)$$

consistently with the more general result Eq. (5.12). The analog of Eq. (5.10) is Eq. (5.6) and

$$\frac{c_e}{r/\rho} \rightarrow \frac{1}{gX\alpha_e}, \quad (5.14)$$

and of Eq. (5.11) is

$$\frac{(\Delta P^*/\text{mPa})}{(r^*\text{mm}^2/\text{mW})} \approx 288\kappa \frac{d(\text{exp})}{d(\text{erf})} \frac{G_g \Delta\alpha}{\alpha_g} \left( \frac{\text{mm}}{Z^*} \right) \left( \frac{T^*}{300 \text{ K}} \right) \times \left( \frac{\lambda^*}{10 \text{ }\mu\text{m}} \right) \left( \frac{408 \text{ kHz}}{\gamma^*} \right), \quad (5.15a)$$

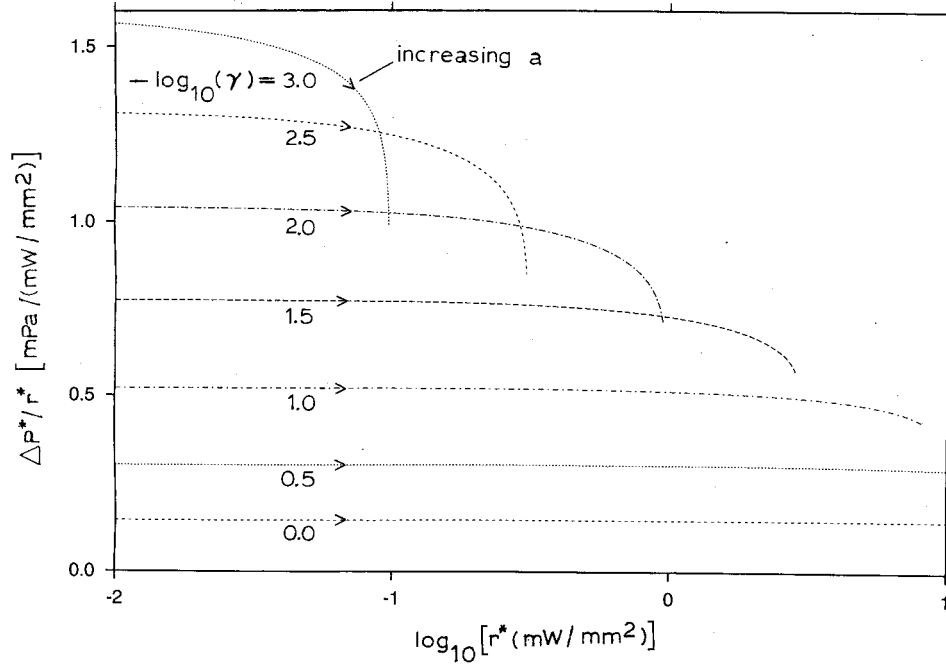


FIG. 3. Dependence on  $r$  of  $\Delta P/r$  for the seven values of  $\gamma$  given by  $-\log_{10}\gamma=0(0.5)3$ : for small  $r$ ,  $\Delta P/r$  is a decreasing function of  $\gamma$ ; as each curve is traced out, starting from  $r=0^+$ ,  $a$  is increasing, and  $r$ , as a function of  $a$ , has a maximum value, evident here for the five smaller values of  $\gamma$ . The parameters are as in Fig. 2 except that  $z=0$  and  $\gamma>0$ .

$$\frac{1000c_e}{(r^*\text{mm}^2/\text{mW})} \approx \frac{5.11}{\alpha_e} \left( \frac{10 \text{ cm}}{X^*} \right) \left( \frac{\text{Pa}}{P^*} \right) \left( \frac{T^*}{300 \text{ K}} \right) \left( \frac{\lambda^*}{10 \mu\text{m}} \right) \times \left( \frac{408 \text{ kHz}}{\gamma^*} \right), \quad (5.15b)$$

$$g \approx \frac{1}{\alpha_e} \left( \frac{\gamma^*}{408 \text{ kHz}} \right) \left( \frac{Z^*}{\text{mm}} \right) \left( \frac{300 \text{ K}}{T^*} \right)^{1/2} \left( \frac{\mu^*}{30 \text{ amu}} \right)^{1/2}, \quad (5.15c)$$

where our standard value of  $\gamma^*$  has been chosen arbitrarily in terms of the standard values of  $Z^*$ ,  $T^*$ ,  $\mu^*$ , that is,

$$(2b^*300 \text{ K}/30 \text{ amu})^{1/2}/\text{mm} \approx 408 \text{ kHz}. \quad (5.15d)$$

For small  $r$ ,  $\Delta P/r$  and  $c_e/r$  are now essentially independent of  $r$ . Figure 3 shows exact results for  $\Delta P/r$  versus  $r$  for seven values of  $\gamma$  using our standard quantities (again excluding  $\Delta P^*$  and  $r^*$ ) and with parameters as in the caption. An interesting saturation effect, that is,  $r$  as a function of  $a$  having a maximum value, is clearly evident for the smaller values of  $\gamma$ , the curves ending as shown. This effect is pursued in Fig. 4, in which the exact  $r$  is shown versus  $a$  for the same conditions as in Fig. 3. That  $c_e$  also must saturate follows from Eq. (5.12), and exact  $c_e$  versus  $a$  is shown in Fig. 5, again for the same conditions.

The convergence of the curves in Figs. 4 and 5 for small  $a$  is a manifestation of the results (3.4), (5.12) and (5.13). Related results for  $z=0$ , which are illustrated in Fig. 5, are readily obtained, for example,  $\lim_{g \rightarrow 0} c_e(a, g) = \frac{1}{2}$ , consis-

tently with Ref. [24], and the value of  $\lim_{a \rightarrow \infty} c_e(a, g)$ . Although of interest mathematically, the limit as  $a \rightarrow \infty$  has no real physical significance because our assumptions would be violated for sufficiently large  $a$ , and analogous remarks apply to parts of the curves shown in Figs. 2–5.

## VI. APPLICATIONS TO EXPERIMENTS

It seems to the present author that rigorous tests of theory should be made via experimental measurements of  $\Delta P$  as a function of  $r$  in order to test the results for SLID displayed in Sec. 5 and illustrated in Figs. 2 and 3. If  $c_e$  were measurable, then other independent tests could be made, as illustrated in Figs. 4 and 5. Such experimental data have not been presented, but differences between predictions of the present theory and of previous theories may be illustrated by the limited comparisons which are possible at present.

Experimental results [12–16] have usually been presented as essentially single values of a quantity denoted by  $\Delta$  and defined by

$$\Delta = (\Delta P/P)/C_e, \quad (6.1)$$

where  $C_e$  (not our  $c_e$ ) is the concentration of excited molecules which have just been excited but have not yet suffered a velocity-randomizing collision, as clearly explained in Ref. [13]. In fact,  $\Delta$  versus  $P$  is shown, but only in order to infer a single free-molecule result for small  $P$ .

A problem with this procedure is that  $\Delta$  itself is not an experimentally measured quantity, but is presumably obtained from *measured* values of  $(\Delta P/P)/r$  by dividing by

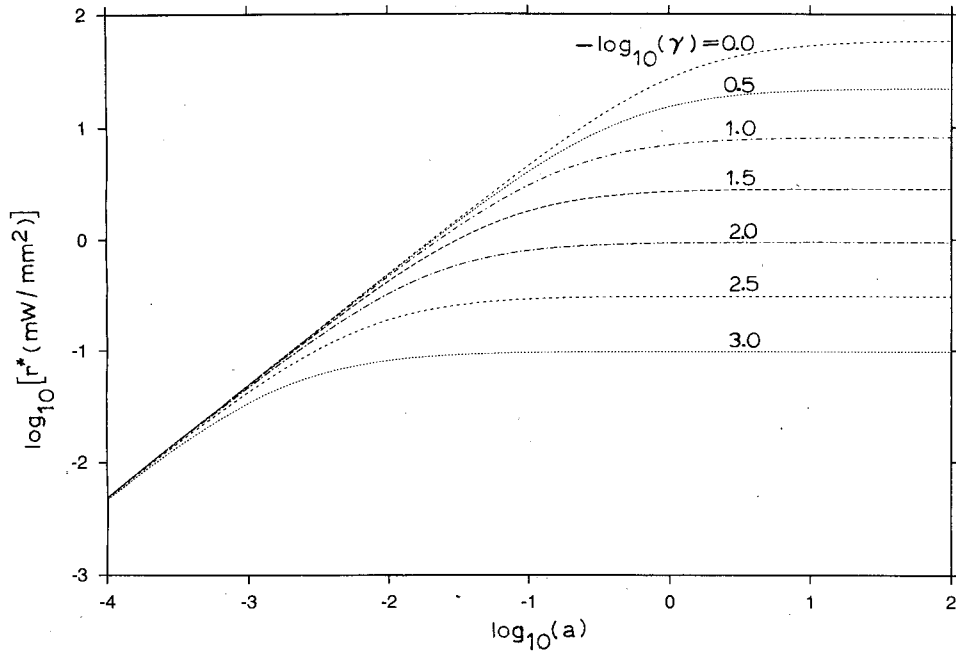


FIG. 4. Dependence on  $a$  of  $r$  for the seven values of  $\gamma$  in Fig. 3;  $r$  is an increasing function of  $\gamma$  for all  $a$ . The parameters are as in Fig. 3.

calculated values of  $C_e/r$ . The present author is not clear as to why this is done, and prefers to renormalize the given values of  $\Delta$  to values of  $\delta$ , defined in Eq. (3.5), in order to use results such as Eqs. (5.6), (5.8), and (5.10) directly. Hence we write

$$\delta = \left( \frac{C_e}{r/\rho} \right) \Delta \tag{6.2}$$

and hope that the values reported [14,16] for  $C_e/(r/\rho)$  are correct; for FP geometry, with  $\nu_k$  assumed negligible, we are told that [14,16]

$$\left( \frac{C_e}{r/\rho} \right) = \frac{\pi^{1/2}}{X} \left( \frac{Y}{1+Y} \right). \tag{6.3}$$

We note that, although our computations have been made for the large- $Y$  limit, we should not simplify Eq. (6.3) to that

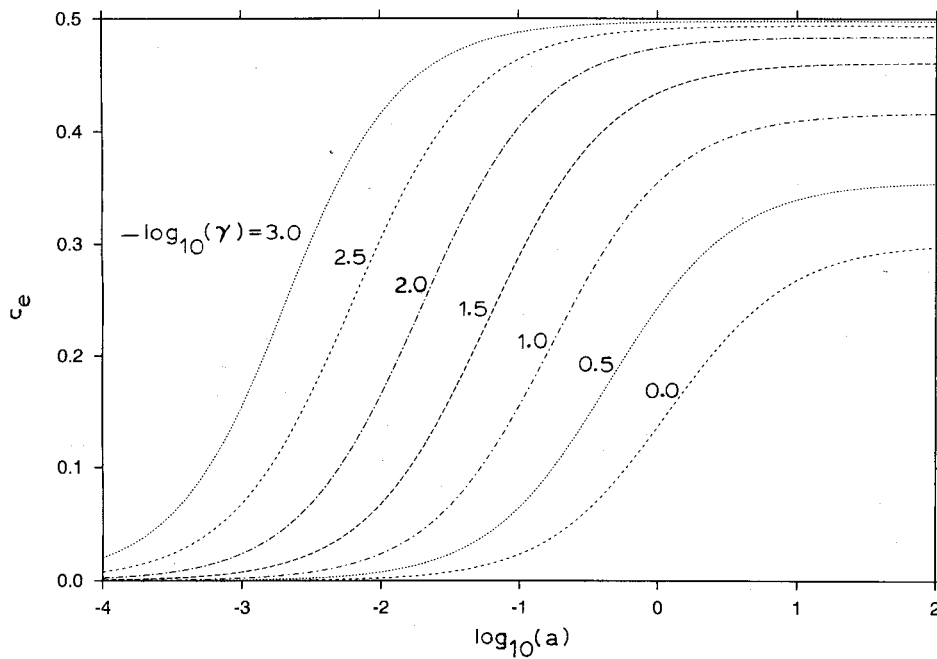


FIG. 5. Dependence on  $a$  of  $c_e$  for the seven values of  $\gamma$  in Fig. 3;  $c_e$  is a decreasing function of  $\gamma$  for all  $a$ . The parameters are as in Fig. 3.

case because it is due to the experimentalists, who use Eq. (6.3) as it stands in order to calculate their  $\Delta$  from Eq. (6.1); thus,  $(1+Y)/Y$  appears different from unity only in the context of translating the results presented in the experimental papers. It follows from Eqs. (6.1)–(6.3) that

$$\Delta = (X/\pi^{1/2})(1+Y^{-1})\delta, \quad (6.4)$$

the important low-intensity special cases of  $\delta$  being given by Eqs. (5.6) and (5.10). To compare specifically to previous work, we write the analog of Eq. (6.4) which is given in Ref. [16], that is,

$$\tilde{\Delta} = \frac{2(1+\varepsilon)\phi(\Omega)X}{\pi^{1/2}} \left( \frac{1+Y}{Y} \right) \tilde{\Delta}\alpha, \quad (6.5)$$

where  $\phi(\Omega)$  is the detuning function and  $\varepsilon$  is a small correction depending on  $Y$  [16]; the tildes have been inserted to avoid confusion with our quantities in Eq. (6.4). For our special case (b') in Sec. VB 3, that is, the case  $g=0$  with small  $a$ , Eq. (5.10a) in Eq. (6.4) gives

$$\frac{1000\Delta\alpha}{\Delta} \rightarrow -\frac{500\pi^{3/2}}{\kappa X(\ln a + \sigma/2)} \left( \frac{Y}{1+Y} \right) \frac{d(\text{erf})}{d(\text{exp})}, \quad (6.6)$$

where we have put  $\alpha_g = \alpha_e = 1$  in the RHS, in accord with experiment [14,16].

Finally, we must interpret  $\kappa$ , and an attempt is presented in Appendix H, based on free-molecule-flow transition-probability calculations. Assuming that it is valid to use Eq. (H5) here, we get

$$\frac{1000\Delta\alpha}{\Delta} \rightarrow -\frac{250\pi}{X} \left[ \frac{\ln(2X) - \frac{1}{2}}{\ln a + \sigma/2} \right] \left( \frac{Y}{1+Y} \right) \frac{d(\text{erf})}{d(\text{exp})} \quad (6.7a)$$

$$\rightarrow -\frac{250\pi^{1/2}}{Xv_L} \left[ \frac{\ln(2X) - \frac{1}{2}}{\ln a + \sigma/2} \right] \left( \frac{Y}{1+Y} \right), \quad (6.7b)$$

where we have used our prescription (5.7) for relating  $d(\text{exp})/d(\text{erf})$  to  $v_L$  to get Eq. (6.7b). Thus, in any estimates of values of  $\Delta\alpha$ , our estimates  $\Delta\alpha$  [Eq. (6.7)] and previous ones  $\tilde{\Delta}\alpha$  [Eq. (6.5)] are related (on putting  $\Delta = \tilde{\Delta}$ ) as

$$\frac{\Delta\alpha}{\tilde{\Delta}\alpha} \rightarrow -\frac{(1+\varepsilon)}{2} \left[ \frac{\ln(2X) - \frac{1}{2}}{\ln a + \sigma/2} \right] \frac{\phi(\Omega)}{v_L}. \quad (6.8)$$

Under general experimental conditions [12–16],

$$\phi(\Omega) \approx v_L, \quad (6.9)$$

resulting in a nice simplification of Eq. (6.8).

We recall that the results (6.6)–(6.8) come from the case  $g=0$  with small  $a$ . For the other special cases (a) and (c') in Secs. VB 1 and VB 5, that is, the cases of small  $a$  with and without  $z=0$ , we should use Eq. (5.6) instead of Eq. (5.10a) in Eq. (6.4) to get the following analog of Eq. (6.8):

TABLE I. Comparison of results from Eq. (6.7) with those from Refs. [14,16] with FP geometry. The  $P(5)\perp$  and  $P(5)\parallel$  transitions are for OCS with molecular angular momentum  $\mathbf{J}$  perpendicular and parallel, respectively, to the surface; the other seven transitions are for  $^{13}\text{CH}_3\text{F}$ . The case  $R(4,3)^*$  used a LiF (001) surface, and the other eight cases used glass surfaces. The values of  $\tilde{\Delta}$  quoted for Ref. [16] have been estimated by the present author, and the corresponding values of  $\tilde{\Delta}\alpha$  recalculated, using  $\varepsilon = -0.06$  rather than [16]  $\varepsilon = 0$ ; the value of  $\tilde{\Delta}\alpha$  quoted [16] for the  $R(4,4)$  transition does not seem to be consistent with Fig. 2 of Ref. [16], and has been reestimated here using the present author's estimate of  $\tilde{\Delta}$ .

Reference	Transition	$-\tilde{\Delta}$	$-1000\tilde{\Delta}\alpha$	$-1000\Delta\alpha$
14	$R(4,3)^*$	0.85	14	6.9
14	$R(4,3)$	0.17	2.8	1.4
16	$R(4,3)$	0.48	2.3	1.4
16	$R(4,4)$	0.70	3.4	2.1
16	$R(4,0/1)$	0.38	1.8	1.1
16	$Q(12,3)$	0.00	0.0	0.0
16	$P(5)\perp$	-0.19	-0.9	-0.6
16	$P(5)\parallel$	0.00	0.0	0.0

$$\frac{\Delta\alpha}{\tilde{\Delta}\alpha} \rightarrow \frac{(1+\varepsilon)}{\pi^{1/2}} \frac{g}{G_g} \left[ \ln(2X) - \frac{1}{2} \right] \frac{\phi(\Omega)}{v_L}, \quad (6.10)$$

which also simplifies nicely with Eq. (6.9).

We now use the FP data of Refs. [14,16] to infer values of  $\Delta\alpha$  and compare them to those  $\tilde{\Delta}\alpha$  obtained therein; we use Eq. (6.9) throughout the working. Reference [14] presents data on the  $R(4,3)$  transition of  $^{13}\text{CH}_3\text{F}$  with both LiF(001) and glass surfaces; the parameters required for Eq. (6.7) are, in both cases,  $v_L \approx 0.50$ ,  $X \approx 105$ ,  $Y \approx 6$ , and  $a \approx 0.010$  from Eq. (5.11c) (in which we use  $r^* = 10$  mW/6 mm<sup>2</sup>,  $P^* = 3.3$  Pa and  $\lambda^* = 9$   $\mu\text{m}$ ), giving  $1000\Delta\alpha/\Delta \approx 8.1$ . Reference [16] contains data on the  $R(4,k):k=0,1,3,4$  transitions of  $^{13}\text{CH}_3\text{F}$  and the  $P(5)$  transition of OCS, all on glass surfaces; now  $v_L \approx 0.6$ ,  $X \approx 265$ ,  $Y \approx 4.2$ , and  $a \approx 0.010$  (coincidentally:  $r^* = 10$  mW/4.2 mm<sup>2</sup> here), giving  $1000\Delta\alpha/\Delta \approx 3.0$ . The comparisons are shown in Table I.

In the author's opinion, although our FP computations may reasonably model FP experiments, at least to a certain degree, they do not correctly model CC experiments. For example, the CC analog of Eq. (6.6) cannot have logarithmic behavior, and it would be meaningless to use a CC interpretation of  $\kappa$  therein. Therefore, we do not compare with CC work in this paper.

## VII. CONCLUSION

Given the model equations (2.10) for LID, we have shown how exact solutions may be obtained. For the case of SLID, we have given explicit exact numerical and analytical solutions, and specialized them to cases of present interest. Differences between the present and previous work have been discussed, and some have been illustrated by limited applications to experiments. However, almost any theory would agree with existing experimental data due to their lim-

ited nature, and to test this or any other theory more rigorously, much more “fine-grained” experimental data are needed, say, on the dependence on absorbed radiation intensity of LID properties.

Our result that, for example,  $\Delta P$  is not necessarily directly proportional to absorbed radiation intensity, even in the limit of low intensity, is of interest, as all previous work has assumed this proportionality; the deviation from proportionality is logarithmic, however, and if correct would no doubt be difficult to detect experimentally. The ideas presented here concerning the interpretation of the transmission parameter  $\kappa$  are also liable to test, but again the deviation from previous results is logarithmic.

Experimenters using FP geometry should bear in mind the large- $X$  and large- $Y$  assumptions made in FP computations; our applications to experiments (Sec. VI) are made with experimental values [14,16] of  $Y \approx 6$  and 4.2, respectively, which are unlikely to be sufficiently large to give reliable comparisons, although the values of  $X \approx 105$  and 265, respectively, are satisfactory.

It is hoped that other geometries and/or BLID will be subjects of future parts of this series of papers.

#### ACKNOWLEDGMENTS

The author is greatly indebted for many time-consuming discussions to Professor A. D. Streater and Professor M. A. Vaksman, whose patience in trying to teach him about LID has seemed endless. He is also indebted to Professor C. B. Collins for several illuminating discussions concerning the analytical properties of the function  $G(u)$ . The work was supported by the Natural Sciences and Engineering Research Council of Canada.

#### APPENDIX A: SOME DISTRIBUTIONS AND INTEGRALS ENTERING THE ANALYSIS

The distributions  $f_d$  ( $d \equiv$  difference) and  $f_s$  ( $s \equiv$  sum) are defined by

$$f_d(\mathbf{v};t) = f_g(\mathbf{v};t) - f_e(\mathbf{v};t), \quad (\text{A1a})$$

$$f_s(\mathbf{v};t) = f_g(\mathbf{v};t) + f_e(\mathbf{v};t). \quad (\text{A1b})$$

We define the following integrals over the distributions, where  $k$  stands for  $g, e, s, d$ :

$$I_{1k}(t) = \int \int \int d^3\mathbf{v} f_k(\mathbf{v};t), \quad (\text{A2a})$$

$$I_{qk}(t) = \int \int \int d^3\mathbf{v} q(v_x) f_k(\mathbf{v};t), \quad (\text{A2b})$$

$$I_{vk}(t) = \int \int \int d^3\mathbf{v} v f_k(\mathbf{v};t), \quad (\text{A2c})$$

$$I_{xk}(t) = \int \int \int d^3\mathbf{v} v_x f_k(\mathbf{v};t), \quad (\text{A2d})$$

$$I_{zk}(t) = \int \int \int d^3\mathbf{v} |v_z| f_k(\mathbf{v};t). \quad (\text{A2e})$$

#### APPENDIX B: DIFFUSE VELOCITY DISTRIBUTION FUNCTIONS

The distributions  $m, M, B$  discussed here are normalized to unity. The usual bulk-Maxwellian distribution  $m(\mathbf{v})$  is well known:

$$m(\mathbf{v}) = \pi^{-3/2} e^{-v^2}. \quad (\text{B1})$$

The analog of Eq. (B1), denoted by  $M(\mathbf{v})$ , for molecules crossing a fixed permeable surface oriented normal to the  $z$  axis, is proportional to  $|v_z| m(\mathbf{v})$  [25], and is accordingly given by

$$M(\mathbf{v}) = |v_z| m(\mathbf{v}) / \langle |v_z| \rangle_m, \quad (\text{B2a})$$

where  $\langle \xi \rangle_m$  stands for the value of  $\xi(\mathbf{v})$  averaged over  $m(\mathbf{v})$  [21]. As  $\langle |v_z| \rangle_m = \pi^{-1/2}$ , we get

$$M(\mathbf{v}) = (|v_z|/\pi) e^{-v^2}. \quad (\text{B2b})$$

For molecules striking buffer particles in the bulk, the analog of Eq. (B1), denoted by  $B(\mathbf{v})$ , is naturally proportional to  $v m(\mathbf{v})$ , and is therefore given by

$$B(\mathbf{v}) = v m(\mathbf{v}) / \langle v \rangle_m. \quad (\text{B3a})$$

As  $\langle v \rangle_m = 2\pi^{-1/2}$ , we get

$$B(\mathbf{v}) = (v/2\pi) e^{-v^2}. \quad (\text{B3b})$$

#### APPENDIX C: DERIVATION OF THE RELAXATION-TIME FORMULA (4.9)

Integration of Eq. (2.10b) with respect to  $\mathbf{v}$  gives

$$\frac{dc_e}{dt} = I_{qd} - (\alpha_{se} z_s \langle |v_z| \rangle_e + \alpha_{be} z_b \theta \langle v \rangle_e + \gamma) c_e, \quad (\text{C1})$$

where  $I_{qd}$ ,  $\langle |v_z| \rangle_e$ ,  $\langle v \rangle_e$ , and of course  $c_e$ , are functions of  $t$ . Putting  $I_{qd} = (c_g - c_e) \langle q \rangle_d$ , we get

$$dc_e/dt = \langle q \rangle_d c_e - c_e/\tau, \quad (\text{C2a})$$

with  $\tau$  defined from

$$\tau^{-1} = \alpha_{se} z_s \langle |v_z| \rangle_e + \alpha_{be} z_b \theta \langle v \rangle_e + \gamma + 2 \langle q \rangle_d. \quad (\text{C2b})$$

Assuming that the distributions  $f_k$  are approximately Maxwellian, then

$$\langle q \rangle_d \approx q_0 (\text{erf} v_b - \text{erf} v_a) / 2 \quad (\text{C3})$$

and Eq. (4.9) follows.

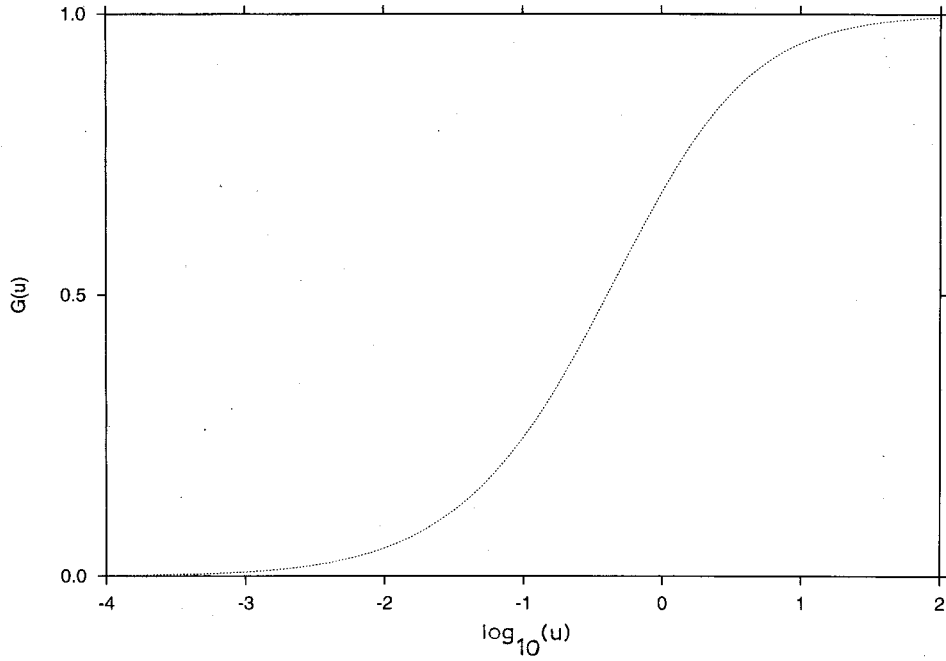


FIG. 6. Our function  $G(u)$  defined in appendix D, in which expansions for small and large  $u$  are given, Eq. (D2) [19].

#### APPENDIX D: THE FUNCTION $G(u)$ AND SOME OF ITS PROPERTIES

The function  $G(u)$  is defined, for  $u > 0$ , by

$$G(u) = \frac{2u}{\pi^{1/2}} \int_0^\infty dx \frac{e^{-x^2}}{(x+u)} \quad (\text{D1})$$

with  $G(0)=0$ , and we include  $G(u)$  under the heading “closed form.” The expansions of  $G(u)$  for small and large values of  $u$  are as follows [19]:

$$G(u) = -\frac{2u \ln u}{\pi^{1/2}} - \frac{\sigma u}{\pi^{1/2}} + 2u^2 + \dots, \quad (\text{D2a})$$

$$G(u) = 1 - \frac{1}{\pi^{1/2}u} + \frac{1}{2u^2} + \dots, \quad (\text{D2b})$$

where  $\sigma (\approx 0.58)$  is Euler’s constant. Thus,  $G(u)$  is continuous for  $0 \leq u < \infty$ , and has limit unity for large  $u$ . We show  $G(u)$  in Fig. 6. A function complementary to  $G(u)$ , denoted by  $H(u)$ , is defined by

$$H(u) = 1 - G(u). \quad (\text{D3})$$

#### APPENDIX E: INTEGRALS IN THE ANALYTICAL SOLUTION FOR SLID WITH FP GEOMETRY

We define  $X_j$  and  $Y_j$  in terms of the eight constants (5.2) as follows:

$$2CDX_j = CB - DA_j, \quad (\text{E1a})$$

$$2CFY_j = CE_j - FA_j. \quad (\text{E1b})$$

Quantities  $a$  and  $g$  are defined by

$$a = Dq_0/C = (\alpha_g + \alpha_e)q_0/\alpha_g\alpha_e, \quad (\text{E2})$$

$$g = F\gamma/C = \gamma/\alpha_e. \quad (\text{E3})$$

A quantity  $d(\exp)$  is defined by

$$d(\exp) = \exp(-v_a^2) - \exp(-v_b^2), \quad (\text{E4})$$

and readers are reminded of the analogous definition (4.10) of  $d(\text{erf})$ . Finally in this development of notation,  $G(a)$ ,  $G(g)$ , and  $G(a+g)$ , and their complementary counterparts, are written in abbreviated forms as follows:

$$G_\xi = G(\xi), \quad (\text{E5a})$$

$$H_\xi = H(\xi), \quad (\text{E5b})$$

where  $\xi$  stands for  $a, g$ , or  $w$ , with  $w$  defined by

$$w = a + g. \quad (\text{E6})$$

With the definitions

$$W_j = (aX_j + gY_j)/w, \quad (\text{E7})$$

$$J = 2 - d(\text{erf}), \quad (\text{E8})$$

the results of calculating the required integrals (Appendix A) may be written as follows:

$$I_{1j} = A_j/C + W_j G_w d(\text{erf}) + JY_j G_g, \quad (\text{E9a})$$

$$I_{qj} = (A_j/2C + W_j G_w) q_0 d(\text{erf}), \quad (\text{E9b})$$

$$I_{xj} = (W_j G_w - Y_j G_g) d(\exp)/\pi^{1/2}, \quad (\text{E9c})$$

$$I_{zj} = A_j/\pi^{1/2} C + w W_j H_w d(\text{erf}) + g J Y_j H_g. \quad (\text{E9d})$$

#### APPENDIX F: EXACT RESULTS FOR THE GENERAL CASE OF SLID WITH FP GEOMETRY

With  $\xi \equiv I_{1e}$ ,  $I_{qd}$ , and  $I_{xs}$ , we write

$$\xi = \xi^{(\text{num})}/\xi^{(\text{den})} \quad (\text{F1})$$

in an obvious notation [21]. With the definitions in Appendix E and the definitions

$$y = \pi^{1/2}(1 - z), \quad (\text{F2})$$

$$\Delta\alpha = \alpha_g - \alpha_e, \quad (\text{F3})$$

$$\Sigma\alpha = \alpha_g + \alpha_e, \quad (\text{F4})$$

$$V = y[wG_g - (g + aG_g)G_w]d(\text{erf})/2, \quad (\text{F5})$$

$$K = z + ygH_g, \quad (\text{F6})$$

the results may be written as follows:

$$I_{1e}^{(\text{num})} = (ywH_gH_w + KG_w + V)a\alpha_g d(\text{erf}), \quad (\text{F7})$$

$$I_{qd}^{(\text{num})} = [K(w - aG_w) + gV]a\alpha_g d(\text{erf}), \quad (\text{F8})$$

$$I_{xs}^{(\text{num})} = (KG_w + V)a\Delta\alpha d(\exp), \quad (\text{F9})$$

$$I_{1e}^{(\text{den})} = 2Kw\Sigma\alpha + \{azG_w\Delta\alpha + y[a(2w\alpha_g - aG_g\Delta\alpha)H_w - g(2a\alpha_e + g\Sigma\alpha)(H_g - H_w)] + aV\Delta\alpha\}d(\text{erf}), \quad (\text{F10})$$

$$I_{qd}^{(\text{den})} = I_{xs}^{(\text{den})}/\pi^{1/2} = I_{1e}^{(\text{den})}. \quad (\text{F11})$$

#### APPENDIX G: EXACT RESULTS FOR THE CASE $g=0$ , $z>0$ OF SLID WITH FP GEOMETRY

With the notation used in Appendix F, the results are Eq. (F11) and as follows:

$$I_{1e}^{(\text{num})} = (zG_a + yaH_a)\alpha_g d(\text{erf})/2, \quad (\text{G1})$$

$$I_{qd}^{(\text{num})} = zaH_a\alpha_g d(\text{erf})/2, \quad (\text{G2})$$

$$I_{xs}^{(\text{num})} = zG_a\Delta\alpha d(\exp)/2, \quad (\text{G3})$$

$$I_{1e}^{(\text{den})} = z\Sigma\alpha + (2yaH_a\alpha_g + zG_a\Delta\alpha)d(\text{erf})/2. \quad (\text{G4})$$

#### APPENDIX H: CHOICE OF THE PARAMETER $\kappa$

We use results from free-molecule-flow, with diffuse surface scattering ( $\alpha = 1$ ), transition-probability calculations for an open cell lying between two equilibrium reservoirs with number-density difference  $\Delta\rho$  and pressure difference  $\Delta P$ . The transmission probability of a molecule across the system is denoted by  $\Psi$ , and the number rate  $dN/dt$  of molecules which cross the cell is given by  $\frac{1}{2}\Psi A\Delta\rho\langle|v_x|\rangle_m$ , that is (Appendix B),

$$dN/dt = \Psi A\Delta\rho/2\pi^{1/2}, \quad (\text{H1})$$

where  $A$  is the flow cross-sectional area. The average velocity of molecules in the cell is  $I_{xs}$  in the  $x$  direction, giving

$$dN/dt = A\rho I_{xs}. \quad (\text{H2})$$

Now Eqs. (3.1), (H1), and (H2) give our interpretation of  $\kappa$  in the form

$$\kappa X = 2\pi^{1/2}/\Psi. \quad (\text{H3})$$

A good compilation of values of  $\Psi$  for several systems/geometries is given by Berman [26]; for our FP geometry [26],

$$\Psi = (\ln(2X) - \frac{1}{2})/X + O(\ln X/X)^2, \quad (\text{H4})$$

where we choose the large- $X$  expansion. We note that  $Y$  is absent because the limit of large  $Y$  is understood. From Eqs. (H3) and (H4) we get

$$\kappa \rightarrow 2\pi^{1/2}/(\ln(2X) - \frac{1}{2}), \quad (\text{H5})$$

and our standard value of  $\kappa$  is that in Eq. (H5) with  $X = 100$ .

- 
- [1] F.K. Gelmukhanov and A.M. Shalagin, Pis'ma Zh. Eksp. Teor. Fiz. **29**, 773 (1979).  
 [2] A.D. Antsigin, S.N. Atutov, F.K. Gelmukhanov, A.M. Shalagin, and G.G. Telegin, Opt. Commun. **32**, 237 (1980).  
 [3] A.V. Ghiner, M.I. Stockmann, and M.A. Vaksman, Phys. Lett. **96A**, 79 (1983).  
 [4] M.A. Vaksman, Phys. Rev. A **48**, R26 (1993).  
 [5] A.V. Ghiner and M.A. Vaksman, Phys. Rev. A **54**, 3270 (1996).  
 [6] M.A. Vaksman and A. Ben-Reuven, Surf. Sci. **287/288**, 196 (1993).  
 [7] M.A. Vaksman, Phys. Rev. A **52**, 2179 (1995).  
 [8] M.A. Vaksman and I. Podgorski, Can. J. Phys. **74**, 25 (1996).

- [9] M.A. Vaksman, Chem. Phys. Lett. **267**, 77 (1997).  
 [10] M.A. Vaksman and J.L. Dahl, Can. J. Phys. **77**, 145 (1999).  
 [11] A.D. Streater and M.A. Vaksman, Can. J. Phys. **78**, 285 (2000).  
 [12] R.W.M. Hoogeveen, R.J.C. Spreeuw, and L.J.F. Hermans, Phys. Rev. Lett. **59**, 447 (1987).  
 [13] R.W.M. Hoogeveen, G.J. van der Meer, and L.J.F. Hermans, Phys. Rev. A **42**, 6471 (1990).  
 [14] G.J. van der Meer, B. Broers, R.W.M. Hoogeveen, and L.J.F. Hermans, Physica A **182**, 47 (1992).  
 [15] E.J. van Duijn, R. Nokhai, L.J.F. Hermans, A.Yu. Pankov, and S.Yu. Krylov, J. Chem. Phys. **107**, 3999 (1997).

- [16] B. Broers, G.J. van der Meer, R.W.M. Hoogeveen, and L.J.F. Hermans, *J. Chem. Phys.* **95**, 648 (1991).
- [17] V.G. Chernyak, E.A. Vintovkina, and I.V. Chermyaninov, *JETP* **76**, 768 (1993).
- [18] V.M. Zhdanov, A.A. Krylov, and V.I. Roldugin, *JETP* **78**, 49 (1994).
- [19] *Handbook of Mathematical Functions*, edited by M. Abramowitz and I. A. Stegun (Dover, New York, 1972), Sec. 27.6.
- [20] F.O. Goodman (unpublished work).
- [21] Throughout this paper,  $\xi$  is a dummy variable.
- [22] Remember that we are using dimensionless quantities giving Eq. (2.6).
- [23] It is here that a 2D model (Sec. II), if BLID is involved, has its advantage; if BLID is not involved (that is, if we have pure SLID), then  $v_y$  integrates out trivially, and the 2D and 3D models are equivalent (with our choice of FP geometry).
- [24] The case  $g = z = 0$  is trivial, for then there is no mechanism for relaxation from the excited state (except via the laser effect  $a$ ), and we naturally get  $I_{1e} = \frac{1}{2}$ ,  $I_{xs} = I_{qd} = 0$ .
- [25] F.O. Goodman and H.Y. Wachman, *Dynamics of Gas-Surface Scattering* (Academic Press, New York, 1976), Chap. 2.
- [26] A.S. Berman, *J. Appl. Phys.* **36**, 3356 (1965). The denominator of the expression for  $Q_2$  for flat plates should read  $L^3 + 3L^2 + 4 - (L^2 + 4)(L^2 + 1)^{1/2}$ .